## Electronic supplementary materials

For https://doi.org/10.1631/jzus.A2500621

# Unveiling the drivers of $PM_{2.5}$ and $O_3$ pollution rebound in Shandong, China during three periods of 2023 by an integrated machine learning method

Gang WANG[1], Sai LIU[1], Kai WANG[2,3], Huijuan MENG[4], Na ZHAO[5], Hanyu ZHANG[6]

[1]*Department of Environmental and Safety Engineering, College of Chemistry and Chemical Engineering, China University of Petroleum (East China), Qingdao 266580, China*
[2]*Shandong Academy for Environmental Planning, Jinan 250101, China*
[3]*Key Laboratory of Land and Sea Ecological Governance and Systematic Regulation, Ministry of Ecology and Environment, Jinan 250101, China*
[4]*Engineering Training Management Center, Jinan Engineering Polytechnic, Jinan 250200, China*
[5]*Environment Research Institute, Shandong University, Qingdao 266237, China*
[6]*Department of Environmental Science and Engineering, Beijing Technology and Business University, Beijing 100048, China*

### S1. Chemical analysis and quality control of $PM_{2.5}$

#### *(1) Chemical analysis*

A quartz filter was placed in the sample bottle, immersed in 25 ml of ultrapure water, soaked for 30 min, and then placed in an ultrasonic cleaner (SK8200B, Shanghai Kudos Ultrasonic Instrument Co., Ltd., China) for ultrasonic extraction for 20 min. The solutions were drawn into syringes, filtered, and injected into an ion chromatography system (ICS-1100; Dionex, USA) at a flow rate of 1.0 mL/min for water-soluble ion analysis. The concentrations of water-soluble ions ($NO_3^-$, $SO_4^{2-}$, and $NH_4^+$) were determined.

Organic carbon (OC) and elemental carbon (EC) concentrations were measured by the thermal/optical carbon analyzer (Model 5L, Sunset, USA). Firstly, OC was volatilized from the samples as the temperature gradually rose from 120 ℃ to 550 ℃ in a non-oxidizing helium atmosphere. Then the analyzer oven temperature was gradually ramped from 550 ℃ to 800 ℃. The optical pyrolyzed carbon is also formed in this process. Carbon in these volatile components was converted into $CO_2$ by oxidant, then converted into $CH_4$ through a converter, and was finally quantified with a flame ionization detector.

The entire process of the blank experiment and replicate analyses of the filter blanks were also conducted. The mean blank values were used as the background concentrations. In addition, the standard solution of component was analyzed using the same method. Calibration curves of the measured components were established. The correlation coefficients of the analysis standard curves for all water-soluble ions and carbonaceous aerosol were higher than 0.999.

#### *(2) Quality control*

*Sampling system*

Before sampling, the cutting head of the atmospheric particulate sampler was cleaned using deionized water, high-purity water, and alcohol in series and then dried in a baking oven (BGZ-240, Shanghai Boxun Medical Biological Instrument Co., Ltd, China) at 120 ℃. The flow rate of the sampler was calibrated before sampling to ensure that the deviation of the flow rate of the sampling system was within 5%.

*Filters*

The quartz filters were baked at 650 ℃ for 4 h in a muffle furnace (SX2-8-10-S, Shanghai Hede Experimental Equipment Co., Ltd, China) before sampling to remove the influence of volatile components in

the filters on weighing. And this method is quite common in other studies (Wang et al., 2023; Zhang et al., 2024a and 2024b). Before and after the sampling, the quartz filters were weighed using an electronic balance with the precision of 0.01 mg after equilibration for 48 h under a constant temperature (20 ± 1 ℃) and relative humidity (50% ± 5%) in a fully automatic constant temperature and humidity precision weighing system (RG-AWS5, Qingdao Rongguang Electronic Technology Co., Ltd, China).

*Sample transportation and storage*

After sampling was completed, wearing gloves, the sampling filter clamp was opened and tweezers were used to clamp the edge of the filter. The filter was removed and put into the filter box and the boxes were put into a low-temperature insulation box. The collected samples were stored in filter boxes during transportation to prevent folding or squeezing. After the samples were transported to the laboratory, the filters were equilibrated and weighed.

## S2. Chemical analysis and quality control of VOCs

Concentrations of Photochemical Assessment Monitoring Station (PAMS) components (including alkanes, aromatics, alkenes, and alkyne) and oxygenated volatile organic compounds (OVOCs) were calculated as follows:

$$C_i = \frac{M_i}{22.4} \times C_{0i} \times \frac{273.15}{273.15 + T} \times \frac{P}{101325} \quad \text{(S1)}$$

where $C_i$ and $C_{0i}$ are the concentrations of component $i$ (μg/m$^3$ and ppbv, respectively), $M_i$ refers to the molecular weight of component $i$, and $P$ and $T$ refer to pressure (Pa) and temperature (℃), respectively. Meteorological data were obtained from state-controlled monitoring stations near the NMHC sampling site in urban Linyi.

Canisters were pre-cleaned and vacuumed using ultra-pure nitrogen ($N_2$, 99.999%) to remove water vapor, air, and organic compounds before sampling. Canisters were checked using the same analytical method to ensure that none of the target components were detected. The PAMS-certified gas and 2, 4-Dinitrophenylhydrazine derivative standard solutions were used to quantify the components. A calibration curve was obtained for each target component at five different concentrations. The correlation coefficients were all above 0.995, indicating good linearity between the integral areas of the peaks and the corresponding concentrations.

## S3. Calculation methods for sulfur oxidation ratio (SOR), nitrogen oxidation ratio (NOR), primary organic carbon (POC), and ozone formation potential (OFP)

The SOR and NOR were used to evaluate the conversion of $SO_2$ and $NO_2$ to $SO_4^{2-}$ and $NO_3^-$, respectively (Chen et al., 2020; Liu et al., 2019; Wu et al., 2020). The calculation formulas are as follows:

$$\mathrm{SOR} = \frac{[SO_4^{2-}]}{[SO_4^{2-}] + [SO_2]} \quad \text{(S2)}$$

$$\mathrm{NOR} = \frac{[NO_3^-]}{[NO_3^-] + [NO_2]} \quad \text{(S3)}$$

where $[SO_4^{2-}]$ and $[SO_2]$ are the amount-of-substance concentration of $SO_4^{2-}$ and $SO_2$, respectively (μmol/m$^3$). $[NO_3^-]$ and $[NO_2]$ are the amount-of-substance concentration of $NO_3^-$ and $NO_2$, respectively (μmol/m$^3$).

The calculation of POC can be described as follows (Ai et al., 2023; Ao et al., 2025).

$$\mathrm{SOC} = \mathrm{OC} - \mathrm{EC} \times (\mathrm{OC/EC})_{\mathrm{min}} \quad \text{(S4)}$$

$$\mathrm{POC} = \mathrm{OC} - \mathrm{SOC} \quad \text{(S5)}$$

where OC and EC are the measured concentrations of OC and EC, respectively (μg/m$^3$). The $(OC/EC)_{min}$ refers to minimum values of the ratios between OC and EC.

The OFP was used to represent the maximum contribution of VOCs components to $O_3$ generation under optimal conditions. The maximum incremental reactivity (MIR) correction value obtained by Carter (2010) was used to calculate the OFP of each VOC component. The calculation formulae were as follows:

$$OFP_i = C_i \times MIR_i \quad \text{(S6)}$$

where $OFP_i$ represents the OFP of component *i* (μg/m$^3$), $C_i$ represents the mass concentration of component *i* (μg/m$^3$) and $MIR_i$ is the maximum incremental reactivity of component *i*.

**Table S1.** RF model performance with different parameters during early spring period (ESP).

| RF | Best | Ⅰ | Ⅱ | Ⅲ | Ⅳ | Ⅴ |
|---|---|---|---|---|---|---|
| $n_{br}$ | 130 | 347 | 452 | 443 | 354 | 120 |
| $d_{max}$ | 15 | 13 | 8 | 10 | 11 | 10 |
| $n_f$ | 6 | sqrt | log2 | sqrt | 5 | 5 |
| $R^2$ | 0.95 | 0.88 | 0.71 | 0.81 | 0.85 | 0.92 |
| RMSE | 5.29 | 8.20 | 12.80 | 10.37 | 9.05 | 6.88 |
| MAE | 2.84 | 5.83 | 9.38 | 7.62 | 6.54 | 4.78 |

$n_{br}$: number of boosting rounds. $d_{max}$: maximum depth of individual decision trees. $n_f$: number/ratio of features considered per split. $R^2$: coefficients of determination. RMSE: root mean square error. MAE: mean absolute error. Units of RMSE and MAE are μg/m$^3$.

**Table S2.** RF model performance with different parameters during autumn harvest period (AHP).

| RF | Best | Ⅰ | Ⅱ | Ⅲ | Ⅳ | Ⅴ |
|---|---|---|---|---|---|---|
| $n_{br}$ | 332 | 197 | 335 | 407 | 241 | 241 |
| $d_{max}$ | 15 | 15 | 15 | 14 | 3 | 12 |
| $n_f$ | 6 | sqrt | log2 | log2 | sqrt | 8 |
| $R^2$ | 0.96 | 0.94 | 0.94 | 0.88 | 0.43 | 0.93 |
| RMSE | 3.24 | 4.10 | 3.88 | 5.59 | 12.24 | 4.28 |
| MAE | 2.11 | 2.93 | 2.76 | 4.08 | 9.76 | 2.99 |

**Table S3.** RF model performance with different parameters during photochemical season period (PSP).

| RF | Best | Ⅰ | Ⅱ | Ⅲ | Ⅳ | Ⅴ |
|---|---|---|---|---|---|---|
| $n_{br}$ | 358 | 351 | 240 | 414 | 445 | 430 |
| $d_{max}$ | 15 | 3 | 13 | 13 | 14 | 4 |
| $n_f$ | 5 | 10 | log2 | sqrt | log2 | log2 |
| $R^2$ | 0.94 | 0.62 | 0.88 | 0.91 | 0.89 | 0.67 |
| RMSE | 8.80 | 24.91 | 14.00 | 12.09 | 13.31 | 23.16 |
| MAE | 6.28 | 19.89 | 11.06 | 9.34 | 10.44 | 18.48 |

**Table S4.** SHAP values and their 95% confidence intervals during ESP.

| Feature | Mean of SHAP (μg/m$^3$) | 95% confidence interval (μg/m$^3$) |
|---|---|---|
| unix | 5.7 | 5.3-6.3 |
| day_of_year | 5.6 | 5.3-6.0 |
| SP | 4.8 | 4.5-5.1 |
| RH | 4.3 | 4.0-4.7 |
| T | 3.8 | 3.5-4.1 |
| $O_x$ | 2.8 | 2.5-3.0 |
| day_of_week | 2.6 | 2.4-2.8 |
| TCC | 2.5 | 2.3-2.7 |
| hour_of_day | 2.5 | 2.3-2.7 |
| SSRD | 2.4 | 2.2-2.6 |
| WS | 2.2 | 2.0-2.4 |
| BLH | 2.1 | 1.9-2.4 |
| TP | 0.9 | 0.8-1.0 |

**Table S5.** SHAP values and their 95% confidence intervals during AHP.

| Feature | Mean of SHAP (μg/m$^3$) | 95% confidence interval (μg/m$^3$) |
|---|---|---|
| day_of_year | 5.8 | 5.4-6.2 |
| unix | 3.7 | 3.5-4.0 |
| SSRD | 2.8 | 2.6-3.0 |
| $O_x$ | 2.7 | 2.5-2.9 |
| SP | 2.5 | 2.3-2.8 |
| RH | 2.5 | 2.3-2.7 |
| T | 2.4 | 2.3-2.6 |
| day_of_week | 2.2 | 2.0-2.4 |
| WS | 1.9 | 1.8-2.1 |
| hour_of_day | 1.7 | 1.5-1.8 |
| TCC | 1.5 | 1.3-1.6 |
| BLH | 1.4 | 1.3-1.5 |
| TP | 0.8 | 0.7-0.9 |

**Table S6.** SHAP values and their 95% confidence intervals during PSP.

| Feature | Mean of SHAP (μg/m$^3$) | 95% confidence interval (μg/m$^3$) |
|---|---|---|
| $O_x$ | 24.2 | 23.1-25.1 |
| hour_of_day | 9.8 | 9.3-10.3 |
| day_of_year | 7.1 | 6.8-7.4 |
| SSRD | 5.6 | 5.3-5.8 |
| SP | 5.4 | 5.1-5.6 |
| RH | 5.2 | 4.9-5.5 |
| WS | 4.9 | 4.7-5.2 |
| BLH | 4.8 | 4.5-5.0 |
| TCC | 4.7 | 4.5-5.0 |
| T | 4.6 | 4.4-4.9 |
| unix | 4.4 | 4.1-4.6 |
| TP | 2.9 | 2.8-3.1 |
| day_of_week | 2.9 | 2.8-3.1 |

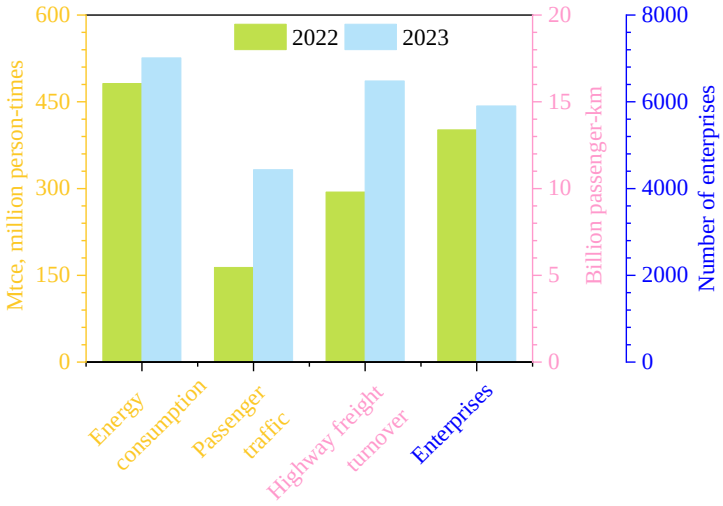


**Fig. S1.** Comparison of energy consumption, passenger traffic, highway freight turnover, and enterprise numbers in Shandong Province (2022-2023). Mtce: million tons of standard coal equivalent.

**References**


Ai J, Qin W, Chen J, et al., 2023. Pollution characteristics and light-driven evolution of environmentally persistent free radicals in $PM_{2.5}$ in two typical northern cities of China. *J. Hazard. Mater.*, 454, 131466. https://doi.org/10.1016/j.jhazmat.2023.131466

Ao Z, Li L, Zhang Y, et al., 2025. Online observation of $PM_{2.5}$ chemical composition in coastal city of the Yangtze River Delta: temporal variation and comparative analysis of pollution types. *Environ. Pollut.*, 383, 126937. https://doi.org/10.1016/j.envpol.2025.126937

Carter WPL, 2010. Development of a condensed SAPRC-07 chemical mechanism. *Atmos. Environ.*, 44, 5336–5345. https://doi.org/10.1016/j.atmosenv.2010.01.024

Chen H, Huo J, Fu Q, et al., 2020. Impact of quarantine measures on chemical compositions of $PM_{2.5}$ during the COVID–19 epidemic in Shanghai, China. *Sci. Total Environ.*, 743, 140758. https://doi.org/10.1016/j.scitotenv.2020.140758

Liu Z, Hu B, Ji D, et al., 2019. Characteristics of fine particle explosive growth events in Beijing, China:

Seasonal variation, chemical evolution pattern and formation mechanism. *Sci. Total Environ.*, 687, 1073–1086. https://doi.org/10.1016/j.scitotenv.2019.06.068

Ministry of Ecology and Environment of the People's Republic of China (MEE), 2017. Ambient air-Determination of inorganic elements in ambient particle matter-Wavelength dispersive X-ray fluorescence spectroscopy (WD-XRF) method (in Chinese). https://www.mee.gov.cn/ywgz/fgbz/bz/bzwb/jcffbz/201705/t20170519_414358.shtml

Wang N, Zhou L, Feng M, et al., 2023. Progressively narrow the gap of $PM_{2.5}$ pollution characteristics at urban and suburban sites in a megacity of Sichuan Basin, China. *J. Environ. Sci.*, 126, 708–721. https://doi.org/10.1016/j.jes.2022.05.017

Wu X, Li M, Chen J, et al., 2020. The characteristics of air pollution induced by the quasi-stationary front: Formation processes and influencing factors. *Sci. Total Environ.*, 707, 136194. https://doi.org/10.1016/j.scitotenv.2019.136194

Zhang J, Sun W, Su Y, et al., 2024a. Chemical composition, sources, and processes of winter haze in Chengdu, China: Insights from integrating the bulk chemical and single particle approaches. *Atmos. Environ.*, 322, 120371. https://doi.org/10.1016/j.atmosenv.2024.120371

Zhang Z, Sha T, Mu Z, et al., 2024b. Changes in sources and formation mechanisms of carbonaceous aerosols driven by short-term air pollution controls in Megacity Xi'an, China. *Atmos. Environ.*, 322, 120369. https://doi.org/10.1016/j.atmosenv.2024.120369